J Mater Sci (2011) 46:2185–2193
DOI 10.1007/s10853-010-5056-5

# Microstructure investigation and thermal stability of 99.1% aluminum processed by equal channel angular extrusion

**Atef Rebhi · Thabet Makhlouf · Yannick Champion · Jean-Philippe Couzinié · Nabil Njah**

Received: 20 August 2010 / Accepted: 4 November 2010 / Published online: 17 November 2010


**Abstract** Microstructure evolution of 99.1% aluminum after equal-channel angular extrusion (ECAE) and subsequent heat-treatment was investigated. After deformation the samples were annealed at different temperatures. The deformed and annealed states were characterized by Transmission Electron Microscopy (TEM), X-ray diffraction (XRD), and microhardness tests. It was shown that the observed microstructure changes during subsequent annealing have to be associated with recovery and cells formation. The initial stages of recovery were investigated using weak-beam technique. The microstructure obtained after annealing for 1 h at 100 °C consists of some arrangements of the dislocations into sub-grain boundaries within the wide preexisting grains. Annealing at 300 °C led to the appearance of a duplex microstructure consisting of bands of slightly coarsened grains associated with refined grains. No growth of dislocation cells was observed up to 400 °C. In XRD measurements, the lattice parameter increase with subsequent heating. This indicates a continuous grain growth during annealing. This is due to the important increase of coherency length, $D$ observed parallel to a substantial decrease of rms-strain, $\varepsilon$.

A. Rebhi (✉) · T. Makhlouf · N. Njah
Laboratoire de Métallurgie Appliquée, Faculté des Sciences de Sfax, BP 1171 (3000), Sfax, Tunisia
e-mail: rebhi_atef@yahoo.fr

Y. Champion · J.-P. Couzinié
Institut de Chimie et des Matériaux Paris-Est (ICMPE), CNRS 2-8 rue Henri Dunant, 94320 Thiais Cedex, France

## Introduction

Equal channel angular extrusion (ECAE), as one of the important severe plastic deformation (SPD) methods, is at present the most promising technique to produce bulk nanostructured and ultrafine-grained materials for structural application [1–3].

During the ECAE process, a metal billet is pressed through a die consisting of two channels with equal cross-section and intersecting at an angle Φ [4–6]. The billet undergoes essentially SPD mainly shearing but retains the same cross-sectional geometry, so that it is possible to repeat the extrusion several times. By multiple pressings, a very large effective shear deformation can be developed in bulk products [4, 5].

In the last two decades, ECAE experiments have mostly focused on the effect of the number of pressings, extrusion route and die shape on the obvious microstructure, and the resulting mechanical or physical properties [7–13].

The mechanical properties and thermal stability are the main concerns for the commercial application of SPD metals. The yield and ultimate tensile stress are significantly enhanced for ultrafine-grained metals processed by SPD techniques compared to their coarse grained counterparts, but they often exhibit low ductility because of the absence of work hardening during subsequent deformation [13]. Furthermore, most ultrafine-grained metals processed by ECAE, especially the high purity metals, are reported to exhibit poor thermal stability, which can limit their commercial application [14, 15]. Both of these properties may be improved by subsequent annealing to modify the microstructure/defects nature of the ultrafine grained materials for further improvement of their mechanical properties and thermal stability.

Recently, many researches have focused on the evolution of microstructures during heating of materials

processed by SPD. Valiev et al. [1] found that the metastable states resulting from SPD followed by heating lead to new unusual properties of the material. Oh-ishi et al. [16] studied the microstructure of an Al–Mg–Si alloy using ECAE combined with heat-treatment, they found that during ECAE the shape of grains was changed, and the aging process was accelerated. Kim et al. [17] studied the effect of ECAE combined with heat-treatment on the hardness of industrial aluminum alloy, and found that the method of pre-ECAE solid-solution treatment combined with post-ECAE ageing treatment exhibited much higher strength. It should be very interesting, therefore, to investigate the annealing behavior of SPD materials with the objective of studying the stability of ECAE-deformed materials especially it has been little studied in the low strain and low temperature regime.

In the present study, the deformed and annealed states were characterized by Transmission Electron Microscopy (TEM), X-ray diffraction (XRD), and Vickers hardness tests. The microstructural changes were recorded and the observed phenomena were analyzed with regard to recovery and associated thermal stability of the material.

## Experimental details

A 99.1% aluminum was used in the present study. The chemical composition is given in Table 1. Prior to ECAE deformation, the material was annealed for 24 h at 500 °C in order to obtain a fully recrystallized homogeneous microstructure. The resulting grain size is about 85 μm. Specimens with (10 × 10) $mm^2$ cross-section and 70 mm length were machined from the annealed ingots. ECAE deformation was carried out at room temperature with a 90° die angle corresponding to a total equivalent strain of about 1 for one passage [18]. After ECAE deformation for one passage, isochronal annealing for 1 h was carried out at various temperatures ranging from 50 to 400 °C.

The microstructures of materials before, after ECAE processing and after subsequent annealing were examined by transmission electron microscopy (TEM) using JEOL 2000EX microscope. For this purpose, samples of 3 mm diameter were obtained by punching and finally thinned by twin-jet electropolishing in a 33% nitric acid and 67% methanol solution at −30 °C under 12 V. The plane X, perpendicular to the longitudinal axis of the pressed sample [3], was chosen for study.

**Table 1** Chemical composition of the investigated material (ppm weight)

| Cr | Cu | Fe | Mg | Mn | Si | Zn | Al |
|---|---|---|---|---|---|---|---|
| 345 | 409 | 3,600 | 1,700 | 385 | 3,500 | 1,900 | Balance |

Hardness changes upon annealing for extruded sample ($N = 1$) were followed by Vickers hardness testing with a load of 1 kg applied for 5 s.

X-ray diffraction was performed on a wide angle diffractometer in the $\theta$–$2\theta$ step scan mode by using Co-K$\alpha$ radiation. Scans were collected over a $2\theta$ range of 20–160° with a step of 0.017°. An acquisition time of 4 s was used at each step to obtain good statistics. The shape of peaks was approximated by the $K\alpha_1 + K\alpha_2$ superposition of a pseudo-Voigt function by using WinPLOTR software; a good agreement is generally found [19].

## Results and discussions

### Microstructure after ECAE

Figure 1 shows TEM micrographs of the microstructure of the undeformed material ($N = 0$). The aluminum of the present investigation contains 0.9% of impurities, mainly iron, silicon, magnesium, and zinc. Iron and silicon are known to form, in aluminum, several ternary compounds unequally rich in silicon. From XRD data and X-ray emission spectrometry coupled with SEM, these precipitates were found to be $Al_8Fe_2Si$ of the hexagonal structure [20]; they are located essentially at the grain boundaries and denoted by letter "P" in Fig. 1a. Figure 1b shows that the undeformed sample contains a low dislocation density. Many of these dislocations are pinned by the precipitates.

After ECAE, the microstructure of deformed material ($N = 1$) shows the presence of almost parallel and elongated grains (Fig. 2a). In addition, newly created subgrains separated by dislocation walls are remarked (Fig. 2b). Moreover, many dislocations are observed at the boundaries as well as inside the "grains". Sub-grains are of about 400 nm in size with many dislocation walls. The contrast difference between the inner part and the outer part of the subgrains shows a bending of the latter indicating a non-equilibrium state. The tendency of grains for bending can be related to size and orientation effects. In order to obtain more detailed information on the dislocation structure of the deformed state, weak-beam (WB) investigations were conducted on selected specimens.

Quantitative analysis of dislocation density in the material could not be performed using TEM micrographs due to presence of too many dislocations highly entangled. Details of microstructural parameters of the material after SPD have been presented in a previous study using XRD measurements [19]. It has been shown that the dislocation density reached $0.5 \times 10^{16}$ $m^{-2}$ after the first pass, the

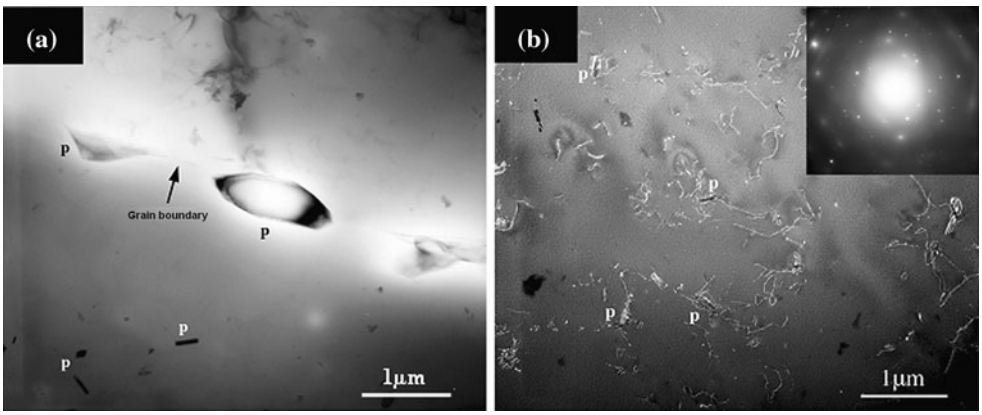


**Fig. 1** TEM images and corresponding selected-area electron diffraction (SAED) pattern of the material without deformation ($N = 0$) (*P* Precipitates)

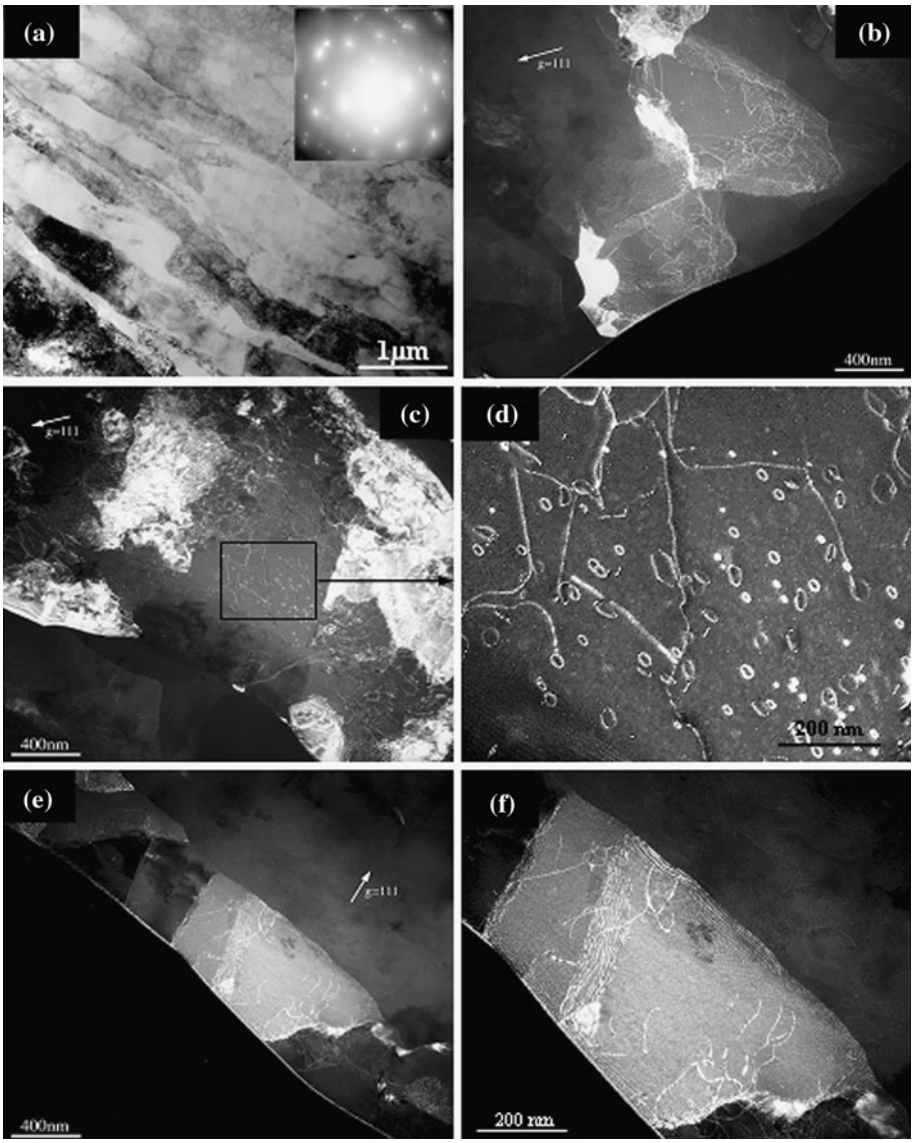


**Fig. 2** TEM micrographs after first pass ($N = 1$): **a** Bright-field image and corresponding SAED pattern; **b–f** A series of weak-beam images

value of coherency length $D$ achieved was 85 nm and the rms-strain $\varepsilon$ was equal to 0.1%.

An important observation consists of the presence of dislocation loops with a diameter of $\sim$15 nm (Fig. 2c, d). The intersection of dislocations on different slip planes often creates vacancies, thus we have the most probable source. Indeed, the stress in the ECAE experiment applied to background of existing dislocations both within the grains and at grain boundaries will continually nucleate and cause dislocations to glide forming the tangles. Intersections between dislocations in these high dislocation density ($\sim 10^{16}$ m$^{-2}$) tangles will subsequently provide localized concentrations of vacancies sufficient to form the loops.

Subgrain boundaries are clear in micrographs as seen in Fig. 2e–f. However, SAED pattern comparison between the two different states ($N = 0$ and $N = 1$) indicates development of higher number of very small subgrains with higher grain boundary misorientation angles in the extruded one.

It has been shown in a previous study [19] that a significant strengthening was achieved after ECAE. In parallel to the increase of $\sigma_{0.2}$, a significant decrease of the hardening exponent is observed after the first pass. Thereafter, a slight increase is observed for route C whereas data points of route $B_C$ do not show any variation. The superior strengthening in the extruded samples is believed to be primarily related to high dislocation accumulation generated by ECAE whereas strain hardening is deeply related to the probability of the emission of dislocations by Frank Read sources. The decrease of the strain hardening in highly deformed materials is due to a saturation density of dislocation. These results are in agreement with those obtained by TEM and XRD experiments.

## Thermal stability

Figure 3 shows TEM micrographs of the microstructure of the ECA extruded material ($N = 1$) and annealed for 1 h at 100 °C. The microstructure (Fig. 3a) is characterized by the appearance of new larger grains in the deformed structure. The annealing at this temperature is associated with a recovery process in which the subgrain boundaries became more clearly delineated. The bright-field image of Fig. 3a is typical of those of severely deformed materials showing a very high dislocation density inside the grains. The WB images shown in Fig. 3b–f are important in providing sharper dislocation contrast at higher magnification. High density of dislocations is retained after this annealing, indicating low recovery activity during this process at 100 °C (Fig. 3b). In this figure, the letter "P" denotes $Al_8Fe_2Si$ precipitates and the symbols "*" show different sub-grains containing many dislocations. Examination of the material in selected region, Fig. 3d shows some arrangement of the dislocations into subgrain boundaries within the 0.5 μm-wide grains. Figure 3e shows that in the same deformed grain there is a presence of subgrains boundaries perfectly formed and others during their formation. In fact, many dislocations are still observed. The micrograph of Fig. 3f shows the early stages of sub-grain boundary formation. The dislocation walls arrowed on the figure are the consequence of dislocation arrangement even though a high dislocation density is still retained nearly. Many dislocations seem to be emetted in the vicinity of subgrains boundaries. The latter acts as a dislocation emission source during further deformation (double arrows).

Annealing at 300 °C for 1 h leads to slightly coarsened structures with an average grain size of about 2 μm as is illustrated in Fig. 4. In this stage, the microstructure is fairly equiaxed. It is also clear from Fig. 4a that there is some poorly resolved substructures within the grains. This annealing led to the appearance of a duplex microstructure consisting of bands of slightly coarsened grains associated with refined grains. Figure 4b shows some arrangement of the dislocations into cells.

Comparatively little is known about the mechanisms of microstructural change during annealing. A non-uniform coarsening leading to the appearance of a duplex microstructure was reported by several authors [13, 21–23]. This is usually attributed to abnormal grain growth, but equally well it can be due to discontinuous recrystallization. Moreover, it appears that the grain structure was not completely stable in the present material since many grain boundaries meet at acute angles and dislocations remain in many of the grains.

The microstructure obtained at 400 °C shows the same behavior to that at 300 °C. No growth of dislocation cells was observed (Fig. 5). However, well resolved grain boundaries are observed indicating an advanced stage of recrystallization (Fig. 5a). The "perfect grains" may arise from a pure recrystallization process, i.e., nucleation and growth, and/or from a duplex microstructure consisting of highly deformed grains in which dislocations or dislocation cells are observed (Fig. 5b), and low-deformed grains; in subsequent heating, the latter grow with the costs of the formers.

Moreover, the material used in this work could have similar temperature annealing behavior as the ECA pressed Al–Mg alloy in which the recovery took place in the temperature range of 100–200 °C. Then the non-equilibrium grain boundaries gradually transform into equilibrium ones in the temperature interval 200–400 °C and finally intensive grain growth was observed above 450 °C [24].

The Vickers hardness, Hv was measured for each sample ($N = 1$) after isochronal annealing, using a diamond pyramidal indentor. Figure 6 shows the variation of Hv with annealing temperature up to 400 °C. Error bar on each

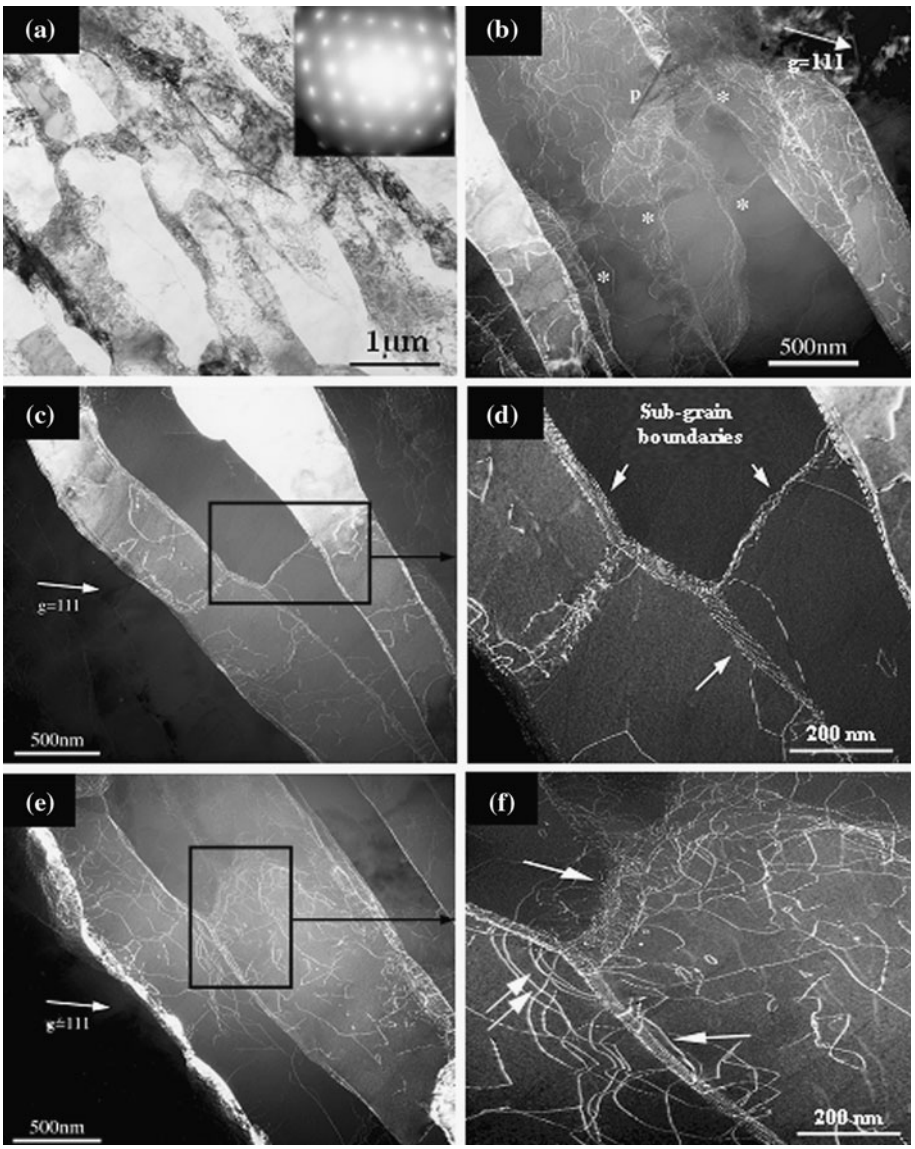


**Fig. 3** TEM images showing ECAE-deformed material ($N = 1$) and annealed for 1 h at 100 °C: **a** Bright-field image and corresponding SAED patterns; **b–f** A series of weak-beam images

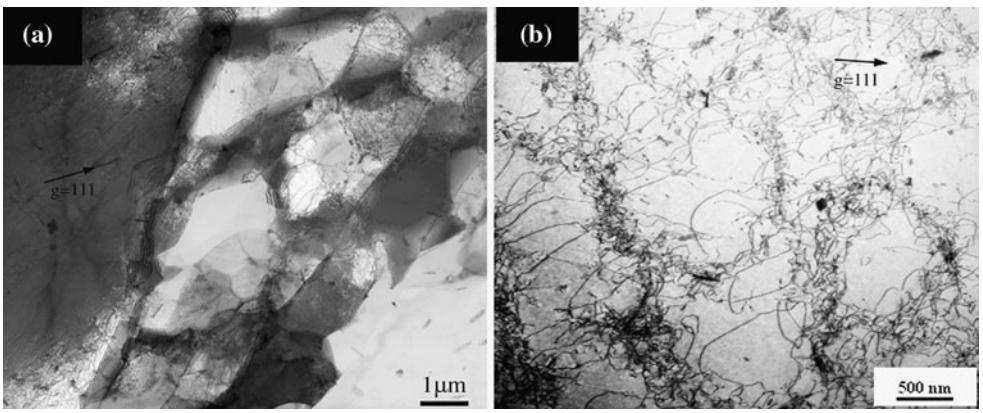


**Fig. 4** TEM images showing ECAE-deformed material ($N = 1$) and annealed for 1 h at 300 °C

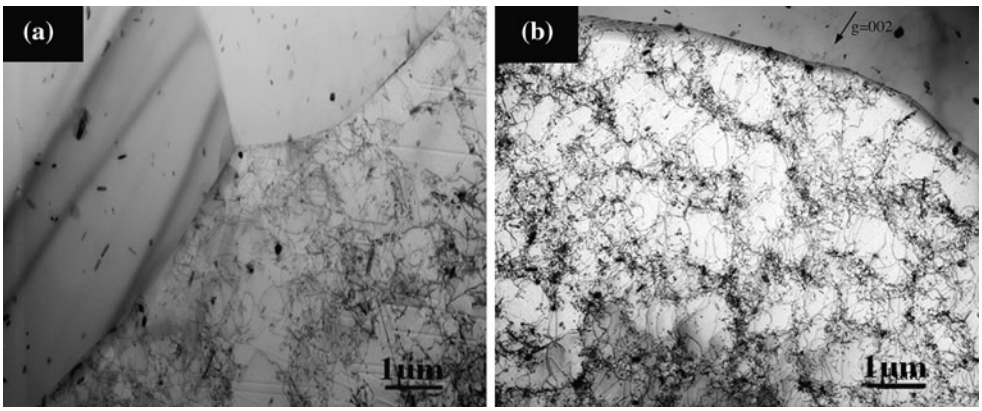


**Fig. 5** TEM images showing ECAE-deformed material ($N = 1$) and annealed for 1 h at 400 °C

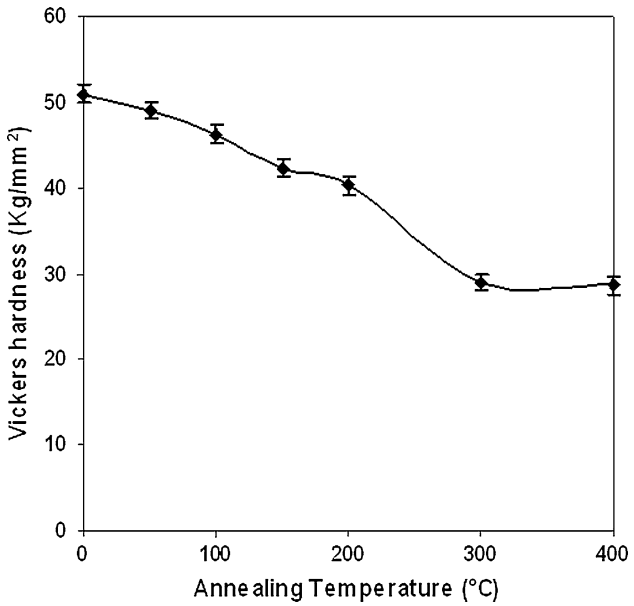


**Fig. 6** Vickers hardness evolution during isochronal annealing for 1 h for extruded samples after one passage

experimental point represents the total range of individual values recorded for Hv in six separate measurements. The plot shows a gradual decrease in the values of Hv with increasing annealing temperature up to 200 °C; a hardness drop is observed between 200 and 300 °C, and stabilization at higher temperatures, 300 °C and above. This result can be explained by the formation of sub-grain boundaries and dislocation walls observed in TEM by anneals at 100 °C. The appearance of a duplex microstructure associated with some arrangement of dislocations into cells explain the hardness fall observed for samples annealed for 200–300 °C. In this temperature range, the material is partially recrystallized. The above observations are in agreement with TEM experiments which reveal that the microstructure recrystallization took place after annealing at 400 °C.

From XRD patterns of the deformed samples ($N = 1$) before and after annealing at different temperatures, three highest intensities were found at (111), (200), and (220) peaks and these were analyses in Fig. 7. The broadening observed in the as-deformed sample was progressively removed by a subsequent annealing. However, the $K\alpha_1$ and $K\alpha_2$ doublet become well resolved around 300 °C, which indicates that the recrystallization was achieved at this temperature. The observed decrease of the peak broadening can be attributed to the decrease of the lattice distortions and the increase of the material grain size. In addition, when the temperature increased, all fundamental peaks are shifted to lower values of $\theta$. Calculated values of the lattice parameter are plotted on Fig. 8, one can see a slight decrease of this parameter up to 150 °C then an important increase for elevated annealing temperature. It should be noted that for low number of passes ($N = 1$), the deformation is located mainly in the outer part of the specimen; the dislocation density is higher than that in the inner part. This applies a compression stress field leading to a decrease of lattice parameter. Since X-ray patterns were recorded on the total surface of the X-plane, the results may depend on which effect is dominant: high dislocation density leading to an increase of the lattice parameter and compression leading to its decrease [25–27]; this may be the reason of the decrease observed below 150 °C. The important value of this parameter obtained toward 300 °C, which correspond to the observed decrease of hardness, indicates the material recrystallization.

XRD measurements enabled us to calculate the coherency length, $D$ (crystallite size) and the rms-strain, $\varepsilon$ (lattice distortions) a function of the temperature, using the Halder–Wagner approach [19]. The obtained results are given on Fig. 9. It should be noted that the parameters calculated from the breadth of peaks are sensitive on the choice of the instrumental breadth $\beta$ins. For a given $2\theta$ value, $\beta$ins was determined using $LaB_6$ as standard reference materials. A strong increase of $D$ is observed toward 200 °C and

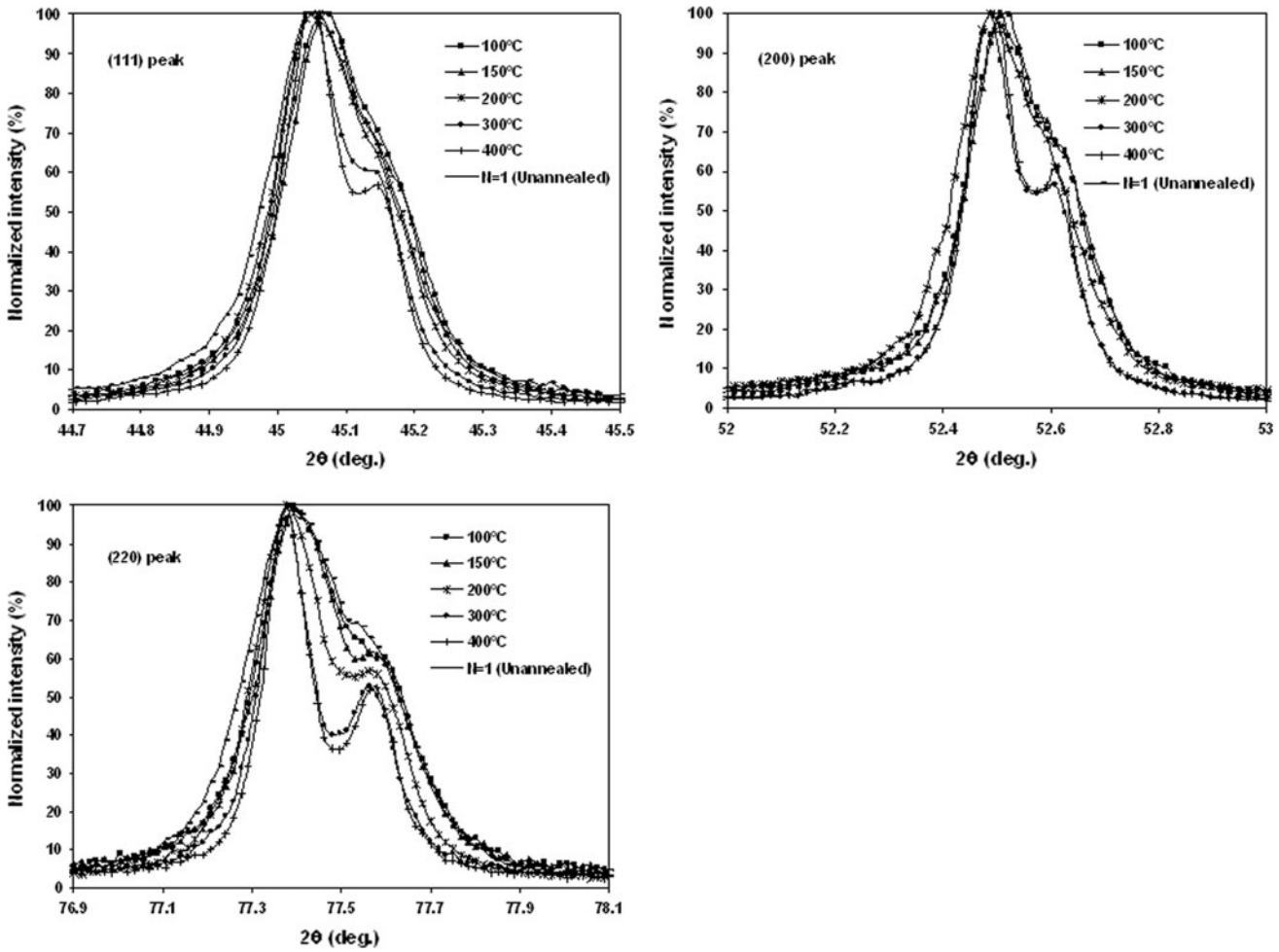


**Fig. 7** The (111), (200), and (220) peaks of the ECA extruded ($N = 1$) material and of the annealed ones scanned in the X-plane

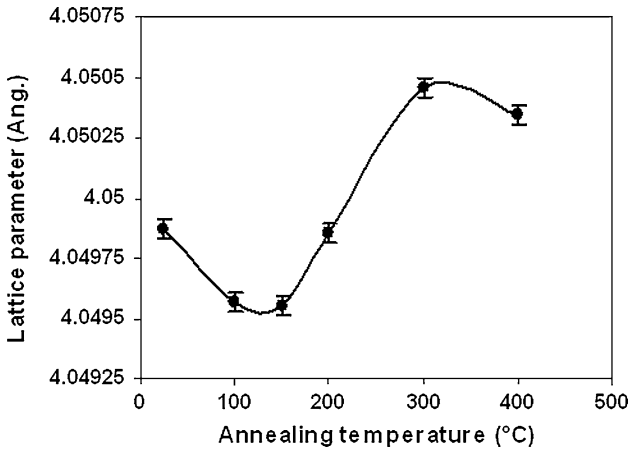


**Fig. 8** Changes of the lattice parameter determined in the X-plane with the annealing temperature

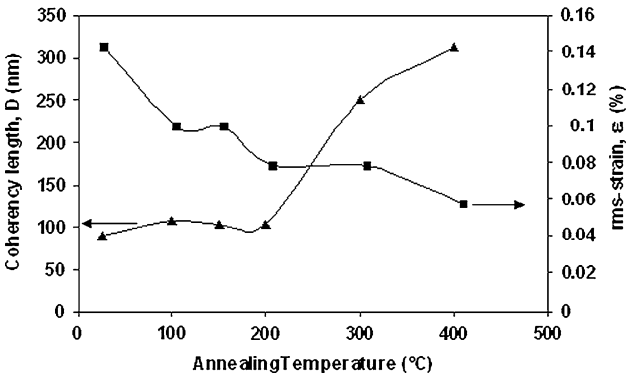


**Fig. 9** Evolution of coherency length, $D$ and of the rms-strain $\varepsilon$ as a function of the annealing temperature

above, parallel to a substantial decrease of $\varepsilon$. This is due to the recovery of microstructure consisting in dislocation annihilation and cell formation. The means of the values after annealing at 400 °C are 312 nm and 0.06% for D and $\varepsilon$, respectively. The reduction of $\varepsilon$ can explain the detected increase of the lattice parameter at this temperature.

The heavy deformation produced by ECAE leads to grain refinement, to values of the order of 85 nm for the present material at strain of $\varepsilon_N = 0.906$ (the calculated value of imposed strain). This microstructure is

characterized, however, by a high dislocation density and newly created subgrains separated by dislocation walls. Annealing leads to several structural changes. The initial loss of dislocations leads to cell formation, and then subgrain walls form. From TEM observations, grain size increases by combinations of grain growth and discontinuous recrystallization, which leads to an inhomogeneous microstructural state.

It has been reported in the literature [28–31] that severely deformed materials can recrystallize continuously during annealing. The conventional recrystallisation concept, however, can hardly be applied to SPD materials, since they contain an unusually high density of deformation-induced defects. The material investigated in the present study provides an example of such a situation. In fact, the dominant process occurring at lower annealing temperatures (100 °C) is the recovery of the grain interiors at almost constant grain size. At higher temperatures (300 °C), the recovered grains begin to grow. The grain growth is accompanied by the presence of dislocation cells as evidenced by a hardness fall. This is a common pattern of microstructural evolution during annealing of SPD processed materials reported in other works [30, 32].

Improvement of the thermal stability of SPD processed nano-structured materials is a crucial problem from the applications point-of-view. Moreover, one of the aims of grain refinement is to enhance plasticity; the main difficulty is to preserve a small grain size at the forming temperature which is close to. In this range of temperature, diffusive transformations are to be considered such as recrystallization. It is then necessary to dragging recrystallization and grain growth; this can be achieved by introducing second phases like precipitates. However, this leads to an increase of the flow stress and a decrease of ductility of the material, and therefore, a limitation of the amount of deformation which can be introduced. The use of low purity metals may be an interesting way since they are relatively easy to work and may retain a suitable grain size at sufficiently high temperatures due to the presence of impurities. In the present investigated material, the presence of $Al_8Fe_2Si$ precipitates delay the diffusion process into the ECA extruded material.

## Conclusion

A 99.1% aluminum was severely deformed by ECAE. The microstructure of ECAE deformed material ($N = 1$) show the presence of almost parallel and long grains which contain a very high density of dislocations. At this stage, ECAE leads to the formation of sub-grains of about 400 nm in size with many dislocation walls. In addition, dislocation loops were observed within the deformed grains.

The microstructural changes observed during annealing were supported by the evolution of hardness. Continuous grain coarsening at lower temperatures led to a gradual hardness decrease and resembled softening due to recovery prior recrystallization. Thereafter, at annealing temperatures above $\sim$200 °C, the softening was more rapid.

The microstructure obtained after annealing for 1 h at 100 °C, contains some arrangement of the dislocations into sub-grain boundaries within 0.5 μm-wide grains. Annealing at 300 °C led to the appearance of a duplex microstructure consisting of bands of slightly coarsened grains associated with refined grains. At 400 °C, a fully recrystallized structure was observed and no growth of dislocations cells was observed.

In XRD measurements, the observed decrease of the peak broadening is attributed to the decrease of the lattice distortions and the increase of the material grain size. In fact, when increasing annealing temperature, an important increase of $D$ is observed parallel to a substantial decrease of $\varepsilon$.

## References


1. Valiev RZ, Islamgaliev RK, Alexandrov IV (2000) Prog Mater Sci 45:103
2. Valiev RZ (2004) Nat Mater 3:511
3. Valiev RZ, Langdon TG (2006) Prog Mater Sci 51:881
4. Segal VM (1995) Mater Sci Eng A197:157
5. Segal VM (2004) Mater Sci Eng A386:269
6. Furukawa M, Horita Z, Nemoto M, Langdon TG (2001) J Mater Sci 36:2835. doi:10.1023/A:1017932417043
7. Yunbin He, Pan Qinglin, Qin Yinjiang, Liu Xiaoyan, Li Wenbin (2010) J Mater Sci 45:1655. doi:10.1007/s10853-009-4143-y
8. Iwahashi Y, Horita Z, Nemoto M, Langdon TG (1997) Acta Mater 45:4733
9. Semiatin SL, Berbon PB, Langdon TG (2001) Scripta Mater 44:135
10. Iwahashi Y, Horita Z, Nemoto M, Langdon TG (1998) Acta Mater 46(9):3317
11. Nakashima K, Horita Z, Nemoto M (2000) Mater Sci Eng A281:82
12. Yamashita A, Yamaguchi D (2000) Mater Sci Eng A287:100
13. Cao WQ, Godfrey A, Liu W, Liu Q (2003) Mater Sci Eng A360:420
14. Wang G, Wu SD, Zuo L, Esling C, Wang ZG, Li GY (2003) Mater Sci Eng A346:83
15. Driver JH (2004) Scripta Mater 51:819
16. Oh-ishi K, Hashi Y, Sadakata A, Kaneko K, Horita Z, Langdon TG (2002) Mater Sci Forum 396–402:333
17. Kim JK, Jeong HG, Hong SI, Kim YS, Kim WJ (2001) Scripta Mater 45:901
18. Iwahashi Y, Wang J, Horita Z, Nemoto M, Langdon TG (1996) Scripta Mater 35:143
19. Rebhi A, Makhlouf T, Njah N, Champion Y, Couzinié J-P (2009) Mater Charact 60:1489

20. Rebhi A, Makhlouf T, Njah N (2009) Phys Procedia 2:1263
21. Yu CY, Sun PL, Kao PW, Chang CP (2004) Mater Sci Eng A366:310
22. Morris DG, Muńoz-Morris MA (2002) Acta Mater 50:4047
23. Mughrabi H, Hoppel HW, Kautz M, Valiev RZ (2003) Z Metallkd 94:1079
24. Wang J, Iwahashi Y, Horita Z, Furukawa M, Nemoto M, Valiev RZ, Langdon TG (1996) Acta Mater 44:2973
25. Zhang K, Alexandrov IV, Lu K (1997) Nanostruct Mater 9:347
26. Lu K, Zhao YH (1999) Nanostruct Mater 12:559
27. Ortiz AL, Shaw L (2004) Acta Mater 52:2185
28. Humphreys FJ, Hatherly M (1995) Recrystallization and related annealing phenomena. Galliard Ltd., Great Yarmouth, Great Britain, pp 7–9
29. Wang G, Wu SD, Zuo L, Esling C, Wang ZG, Li GY (2003) Mater Sci Eng A 346:83
30. Prangnell PB, Bowen JR, Berta M, Apps PJ, Bate PS (2004) Mat Sci Forum 467–470:1260
31. Humphreys FJ (1997) Acta Mater 45:4231
32. Wejrzanowski T, Kurzydyowski KJ (2005) Solid State Phenom 101–102:315